Molecular Imaging

DOI: 10.1002/anie.201103991

Imaging and Quantifying Chemical and Physical Properties of Native Proteins at Molecular Resolution by Force–Volume AFM**

*Izhar Medalsy, Ulf Hensen, and Daniel J. Muller**

Atomic force microscopy (AFM) opened the door to the nanoworld and has developed into multifunctional nanotool in biological research.[1] Currently, AFM is routinely used for high-resolution imaging of native proteins in aqueous solution and at physiological temperature.[1b] Time-lapse AFM imaging allows the observation of single membrane proteins working,[2] rotating,[3] and diffusing.[4] In the force spectroscopy mode, AFM detects interactions ranging from those of single peptides, to proteins and living cells.[1b,5] When combining AFM imaging and force spectroscopy such chemical and physical interactions can be mapped onto the biological object.[5a,c] However, the spatial resolution of such AFM-based combinations is limited to around 50 nm, which is insufficient to either observe structural details or to map physical and chemical properties of single proteins. Recently, force-spectroscopy-based AFM imaging[6] has been revitalized to record arrays of force–distance (F–D) curves at around 4000 times higher speed and at sufficient precision (0.5 nm) for high-resolution imaging. Importantly, force sensitivity achieved (ca. 10 pN) allows the chemical and physical properties of soft biological samples to be measured in their unperturbed state. To date, however, such high-resolution force–volume images of native proteins have not been demonstrated.

Compared to AFM oscillation-mode approaches,[7] a better understanding of local interactions of complex protein assemblies can be gained using F–D curves (Supporting Figure S1).[1b,5a,c,6b] This is because such interactions, being composed of Van der Waals, electrostatic, chemical, and mechanical forces, have different spatial dependencies.[8] Because of their simplicity, F–D curves have been used since the early 1990s to probe specific and unspecific interactions of biomolecular systems.[6b,9] Herein we introduce high-resolution force–volume AFM imaging of the native purple membrane (PM) from *Halobacterium salinarum*. PM consists of the light-driven proton-pump bacteriorhodopsin (BR) and lipids. During the photocycle BR goes through conformational changes and creates a proton gradient across the cellular membrane that is used to power cellular processes.[10] Measurements show that proton transfer along the PM surface is much faster than proton exchange to the bulk water.[11] This unique property that kinetically traps protons is facilitated by the asymmetric physical and chemical properties of PM surfaces. PM has become a reference protein membrane for AFM because of its commercial availability and exceptional stability.[12] High-resolution (ca. 0.5 nm) contact-mode AFM of BR revealed extracellular polypeptide loops changing their conformation with the membrane protein assembly and cytoplasmic loops undergoing force-induced conformational changes.[13]

Using force–volume AFM we imaged PM adsorbed onto freshly cleaved mica in buffer solution. For every pixel of the AFM topography we recorded a F–D curve approaching and retracting AFM tip and PM (Supporting Information 1). The maximal force (trigger force) applied in these approach–retract cycles was limited to 100 pN. When reaching the trigger force the distance travelled by tip and sample was taken to reconstruct the topography. All other imaging and feedback loop parameters were adjusted as described in the Experimental Section. PMs oriented with their cytoplasmic surface towards the buffer solution protruded (7.5 ± 0.5) nm ($n = 20$; $n =$ number of measurements) from the mica surface, whereas PMs exposing their extracellular surfaces protruded (8.3 ± 0.5) nm ($n = 20$; Figure 1a). From the F–D curves recorded we extracted the Young's modulus of elasticity,[14] sample deformation, adhesion force, energy dissipation, and trigger force error (Figure 1b and (Supporting Information 1). The Young's moduli of both PM surfaces were (10 ± 5) MPa ($n = 20$). This compares well to the Young's moduli determined for the cytoplasmic (7 MPa) and to lesser extent to that determined for the extracellular (35 MPa) PM surface by torsional harmonic cantilevers.[7b]

The deformation channel reveals the mechanical response of PM to the AFM tip (Figure 1c). In contrast to the Young's modulus, which is derived from the retraction F–D curve, the deformation is recorded from the approach F–D curve (Supporting Information 1). Thus, both properties are acquired independently. Overview images recorded at a trigger force of approximately 100 pN show a deformation of (1.0 ± 0.5) nm ($n = 40$) of both PM surfaces. Cytoplasmic and extracellular heights measured for PM (Figure 1a) exceed the structural thickness of native, unperturbed PM (ca. 5.6–6.0 nm) by approximately 1.9–2.6 nm.[15] Because of long-range electrostatic double-layer (EDL) repulsion between AFM tip and PM surface the apparent height measured by AFM can be larger than the PM thickness.[15a] At an electrolyte concentration of 150 mM KCl (pH 7.6) of the imaging buffer, the repulsive EDL forces reach around 100 pN when the AFM tip and PM are separated by 2–3 nm.[15a] This repulsive EDL force increases with the surface

[*] Dr. I. Medalsy, Dr. U. Hensen, Prof. Dr. D. J. Muller
ETH Zürich, Dept of Biosystems Science and Engineering
4058 Basel (Switzerland)
E-mail: daniel.mueller@bsse.ethz.ch

[**] This work was supported by ELSO, EMBO, KTS, and SNF. We thank C. Bippes, M. Pfreundschuh, and G. Büldt for their support.
AFM = atomic force microscopy.

Supporting information for this article is available on the WWW under http://dx.doi.org/10.1002/anie.201103991.

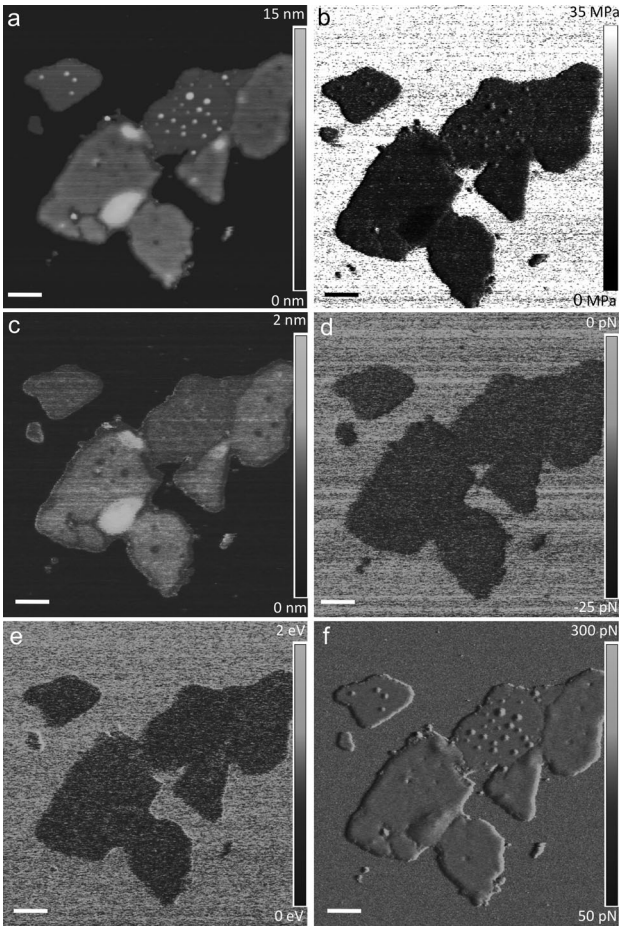

Figure 1. Native purple membrane (PM) observed in buffer solution using force–volume AFM. a) Topography of PMs showing their extracellular and cytoplasmic surface (white areas). b) Young's modulus, c) deformation, d) adhesion force, e) energy dissipation, and f) trigger-force error. Scale bars, 200 nm.

charge density of the PM and the AFM tip.[15a,16] Because the negative surface charge density of the extracellular PM surface is slightly higher than that of the cytoplasmic surface, it repels the tip more and the AFM detects a slightly larger height. By enhancing the trigger forces to overcome the EDL repulsion, the PM height measured approaches the structural PM thickness, however the deformation measured increases (Supporting Information 2). In this case, the deformation measured is (1.9 ± 0.5) nm and (2.3 ± 0.5) nm for the cytoplasmic and extracellular surface, respectively. Thus, the deformation-channel has recorded the EDL interactions between the protein membrane and AFM tip and not the structural deformation. However, at trigger forces significantly higher than the EDL repulsion the deformation maps will reveal structural components more prominently.

The adhesion force channel showed an attractive force of (-10 ± 5) pN ($n = 20$) between the AFM tip and both PM surfaces (Figure 1 d). This force is smaller than that required to rupture the bonds between most ligand and receptor pairs.[5c] The energy of approximately 1 eV ($n = 20$; Figure 1 e) dissipated between AFM tip and PM was the same on both PM surfaces and is in the range corresponding to a few hydrogen bonds (ca. 80–430 meV).[8] The trigger force error channel recorded the deviation (force error) of the AFM feedback loop in adjusting the trigger force (Figure 1 f). This error remained constant over the PM surface except at the rim where the interaction between tip and sample changed drastically.

To observe the structural details of PM contributing to these values we performed force–volume AFM at higher resolution. At a lateral resolution approaching 1–1.5 nm, BR trimers were clearly observed in AFM topographs of the extracellular surface (Figure 2 a). The cross-correlation averaged topography (Figure 2 a) reveals the typical substructure of the BR trimer with three major and three minor protrusions.[13] This agreement with previously achieved AFM, X-ray, and electron microscopy data of BR demonstrates that high-resolution force–volume AFM imaging is capable of observing native protein structures.[15b] Simultaneously to the topography, several physical parameters can be measured using F–D curves (Supporting Information 1). At first glance, the deformation channel did not contain information (Figure 2 b). We used the position and angular orientation of every BR trimer imaged in the AFM topography to define where to extract "unit cells" from the deformation channel (Supporting Information 3). These "unit cells" were superimposed and their average (Figure 2 b) calculated by adding their deformation channel information. This "reference-free" average reveals the formerly masked information of the deformation channel and shows that BR trimers were less deformed ((0.2 ± 0.1) nm) than their surrounding lipids ((1.0 ± 0.1) nm; $n = 200$). However, as stated for the AFM overview images (Figure 1), both electrostatic repulsion and structural deformation may contribute to the deformation. Like the deformation channel, the other channels recorded were noisy and required averaging to reveal further information (Figure 2 c, d). Mapped onto the structural model of PM (see Figure 4 a–c) these averages localized experimentally determined parameters. The adhesion force channel suggests that lipids adhered more to the AFM tip ((-10 ± 5) pN; $n = 200$) than BR ((0 ± 5) pN). This difference may be attributed to asymmetric distributions of Van der Waals forces. Normally, Van der Waals forces are stronger when a tip contacts a flat surface (lipids) than a corrugated surface (BR trimer), which provides less contact area.[8] The Young's modulus shows that the PM lipids ((10 ± 5) MPa; $n = 200$) are much softer than the BR trimers ((30 ± 5) MPa; Figure 2 d, 4 c).

The trigger-force error showed maxima when the AFM tip approached the extracellular protrusions (Supporting Information, Figure S4e) and challenged the AFM feedback loop. Since these errors were very small ($(\pm 8$–$10)$ pN) their impact on the imaging process can be neglected. This highlights the sensitivity of force–volume AFM contouring protein surfaces. To further enhance the resolution of force–volume AFM images, the feedback loop needs to be improved. The energy dissipation channel (Supporting Information Figure S4f) shows that the energy transferred between AFM tip and PM is maximal ((600 ± 200) meV; $n = 500$) at the highest BR protrusion and minimal ((200 ± 200) meV) at the lipid surface.

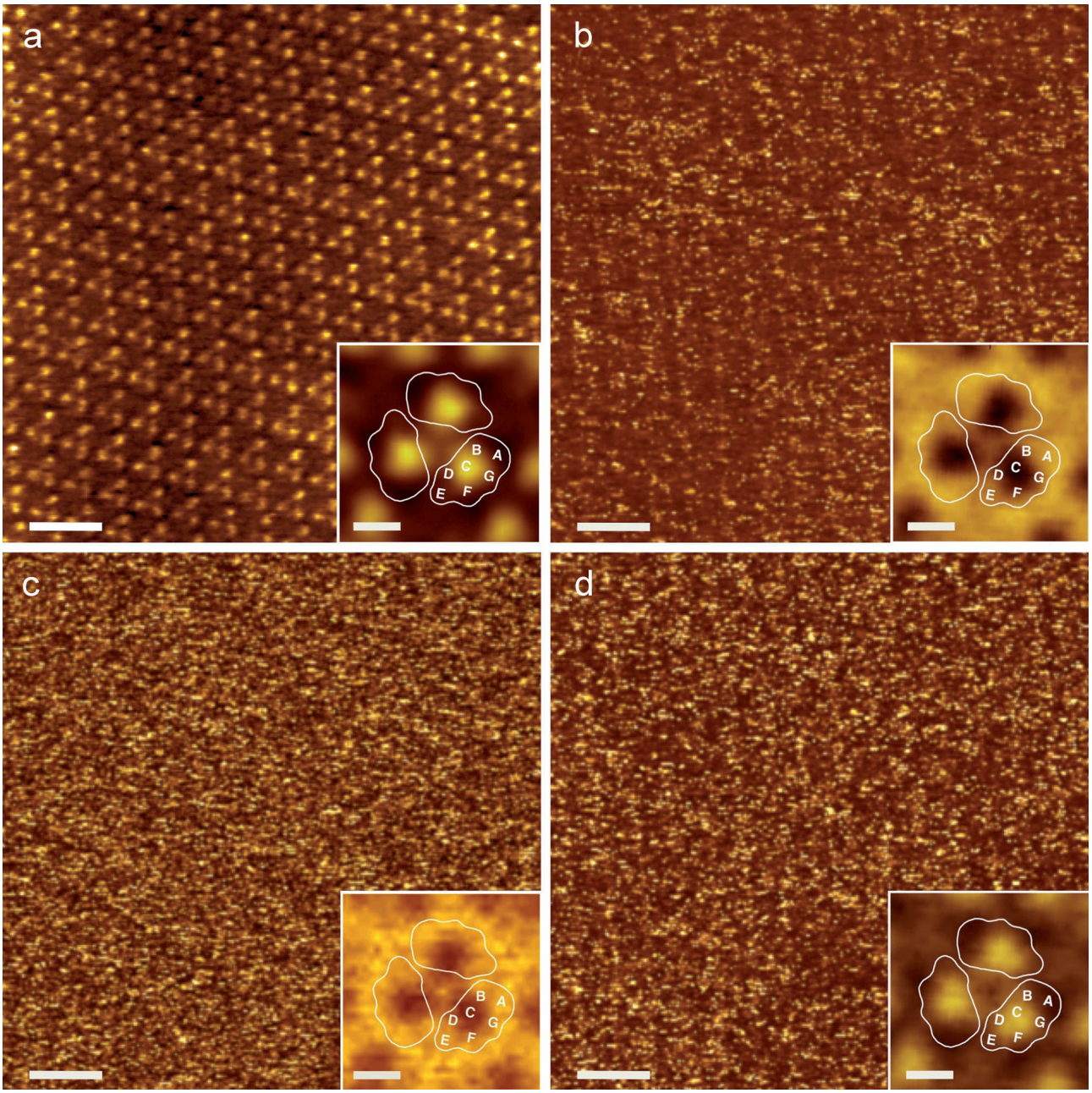

Figure 2. High-resolution force–volume AFM of the extracellular PM surface. a) Topography, images of b) deformation, c) adhesion force, and d) Young's modulus channel. Inset of (a) shows three-fold symmetrized cross-correlation average ($n = 200$) of the bacteriorhodopsin (BR) trimer. Insets of (b–d) show averages of channels (Supporting Information 3). Outlined BR shapes (white lines with the seven transmembrane α-helices A–G indicated) were obtained from X-ray and electron crystallographic analyses.[15b] Full color scales correspond to vertical ranges of a) 1.0 nm, b) 1.2 nm, c) 55 pN, and d) 4 MPa. Scale bars, 10 nm (raw data) and 2 nm (insets).

At high-resolution, the cytoplasmic PM surface showed two distinct conformations (Figure 3). Imaged at low trigger force of 75 pN, polypeptide loops protruded from every BR trimer (Figure 3a, 4d; $n = 500$). These loops were not observed at trigger forces of 125 pN, instead the underlying scaffold of BR trimers became visible (Figure 3d, 4g). This fully reversible force-induced conformational change of the polypeptide EF loop connecting transmembrane α-helices E and F has been observed before.[2a,13] The additional channels revealed further insights (Figure 3, 4d–i). At low force, the EF loop had a much higher Young's modulus ((30 ± 5) MPa) than the surrounding lipids ((10 ± 5) MPa; $n = 500$; Figure 3c, 4f).

At low trigger force, the deformation ranged from (0.4 ± 0.2) nm above the EF loop to (1.0 ± 0.2) nm above lipids ($n = 500$; Figure 3b, 4e). As expected, electrostatic repulsion and structural deformation may contribute to these values. The AFM topography shows hardly any deformation of the EF loop when compared to the PM model (Figure 4j). In this case, the deformation channel appears to reveal electrostatic repulsion between AFM tip and PM. Because the AFM tip is

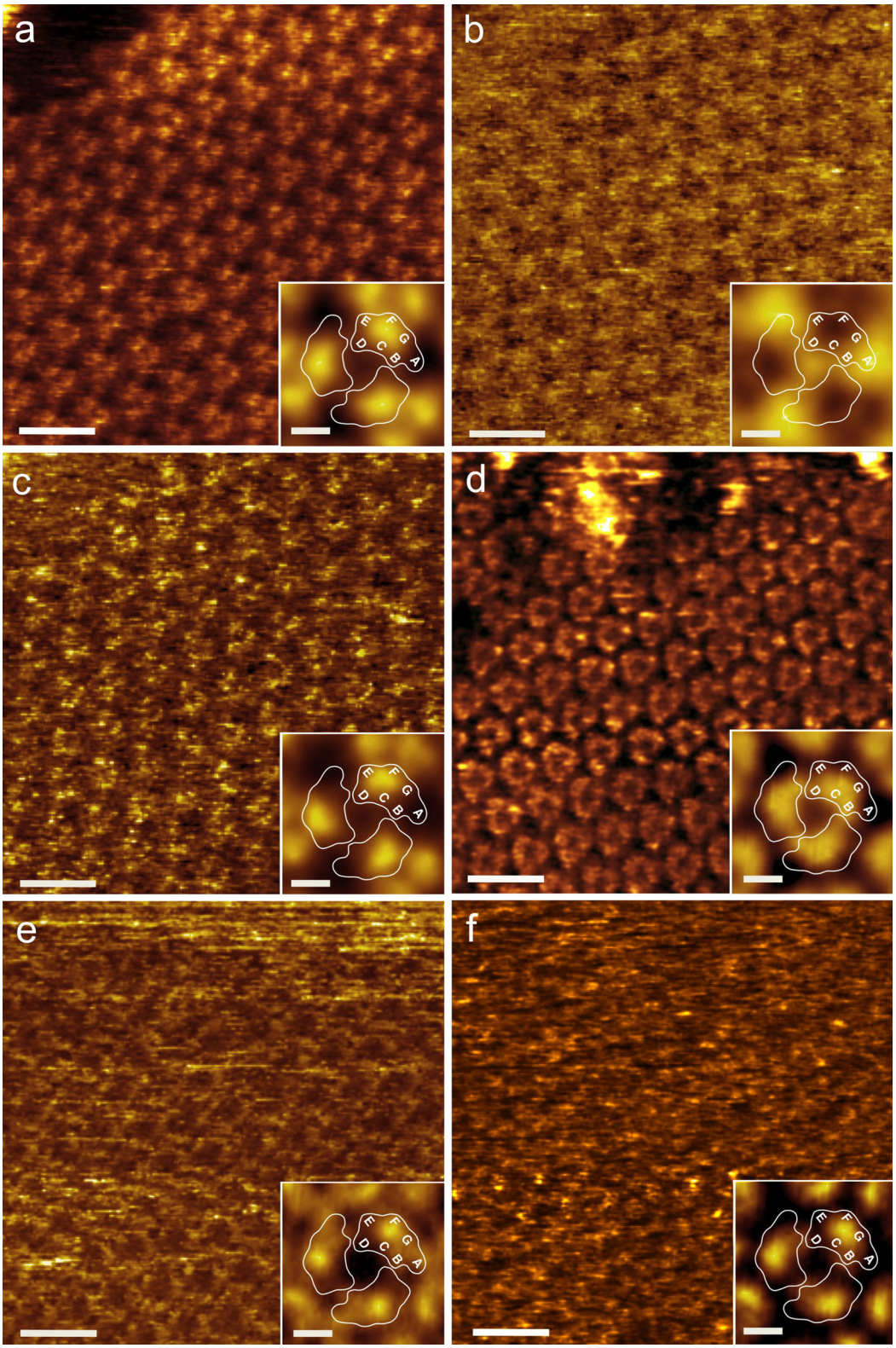

Figure 3. High-resolution force–volume AFM of the cytoplasmic PM surface. a) Low-force topography, and images b) deformation and c) Young's modulus channels. d) High-force topography and images of e) deformation and f) energy dissipation channels. Insets show three-fold symmetrized averages of each channel. Outlined BR shapes (white lines with the seven transmembrane α-helices A–G indicated) were sections close to the cytoplasmic surface obtained from X-ray and electron crystallographic analyses.[15b] Full color scales correspond to vertical ranges of a) 1.2 nm, b) 0.8 nm, c) 6.5 MPa, d) 1.0 nm, e) 1.1 nm, and f) 400 meV. Scale bars, 10 nm (raw data) and 2 nm (insets).

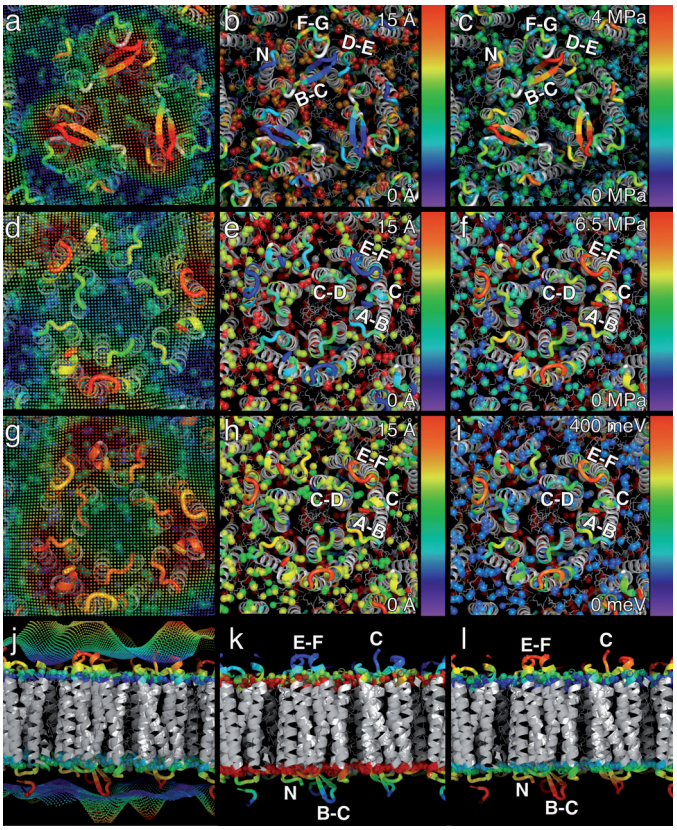

Figure 4. Mapping parameters probed by force–volume AFM onto PM. a) AFM topography, b) deformation channel, and c) Young's modulus (Figure 2) of the extracellular surface. d) Topography, e) deformation channel, and f) Young's modulus of the cytoplasmic surface recorded at low force (Figure 3). g) Topography, h) deformation channel i) and energy dissipation of the cytoplasmic surface recorded at elevated force (Figure 3). j–l) Side views of the PM model and j) AFM topography, k) deformation channels, and j) Young's moduli. Loops connecting transmembrane α-helices A–G and the C- and N-terminal ends of BR are indicated. BR and lipids are color coded based on the force–volume channels. Color scale bars provide quantitative signal information of the colored structural regions. The structural model of PM was generated as described in the Supporting Information.

slightly negatively charged the 'deformation' map suggests that the lipid surface was more negatively charged than that of BR.[9,15a] This changed at higher trigger force when the EF loop deformed by (0.9 ± 0.2) nm while the lipid deformation remained at (1.0 ± 0.2) nm ($n = 500$; Figure 3e, 4h). Now, the channel detected the reversible force-induced deformation of the EF loop.[13]

The deformation of cytoplasmic BR and PM lipids at given trigger forces allows their spring constants k to be estimated as 0.14–0.19 $N\,m^{-1}$ and 0.75–1.25 $mN\,m^{-1}$, respectively. The extracellular surface of BR and lipids reveal k values of 0.50 $N\,m^{-1}$ and 1.00 $mN\,m^{-1}$, respectively. These k values of BR are in very good agreement to elastic neutron scattering approximating 0.12 $N\,m^{-1}$ on the cytoplasmic and 0.33 $N\,m^{-1}$ on the extracellular surface.[17] Thus, lipids show similar mechanical properties on both PM surfaces whereas the proton pump is mechanically softer on the cytoplasmic surface. The mechanical anisotropy of BR allows conformational changes at the cytoplasmic surface that are associated with proton transfer along its pathway through the membrane.[10b,17] The stiffer core of the extracellular BR half could harness the isomerization of retinal to provide the valve function for vectorial proton transfer. Complementary, the lower k values of lipids provides a flexible framework that allows the proton pump to undergo conformational changes necessary for proton pumping. Together, the mechanical anisotropy of BR and PM lipids suggests an evolutionary structural selection with relation to function.[17]

Similarly to the deformation maps, the Young's moduli recorded for both PM surfaces indicate lipids being much softer than BR (Figure 2–4). In agreement, lipids deformed more than BR (Figure 4b,e). In biological membranes flexible lipids are thought to structurally adapt to rigid proteins whereas flexible membrane proteins structurally adapt to more rigid lipids.[18] Thus, the question whether a membrane protein adapts to lipids or vice versa must be specifically solved for each protein membrane. The different elastic properties of lipids and BR (Figure 4c,f) quantifies that in PM lipids structurally adjust to BR. Indeed high-resolution models of BR show PM lipids structurally adapting to the proton pump.[19]

Deformation and Young's modulus maps of PM show that loop EF was the most rigid structure of the cytoplasmic surface (ca. 25 MPa; Figure 3c). This changed when the trigger force was sufficient (ca. 125 pN) to induce collapse of the loop (Figure 3d).[13] The energy dissipated when imaging this conformation was approximately 400 meV (Figure 3f, 4i), which is approximately the energy of one to four intramolecular hydrogen bonds.[8] In its collapsed state the EF loop again exposed the lowest deformability of the PM surface (Figure 3e, 4h). Thus, loop EF appears to be quite stiff and once its stability is overcome it collapses to again adopt a structure of high rigidity (Supporting Information Figure S4k).

Previous AFM experiments showed that loop EF can adopt many conformational states ranging between the fully extended and fully collapsed state.[13,20] This variety of conformational states indicates that the loop is structurally flexible. We have determine the unique mechanical stability of the extended and the collapsed conformational states of loop EF. This explains why the flexible loop EF is well resolved in most structural investigations.[10b] Such a feature has consequences for the function of BR: At low distortions, loop EF remains stiff and holds the functionally important α-helices E and F in place. If structural distortions become sufficiently large, such as by the photoisomerization of the all-*trans* retinal, the loop can adopt alternate conformations that allow α-helices E and F to tilt and proton translocation to take place.[10,21]

Using PM we demonstrate that force–volume AFM is capable of giving high-resolution (1–1.5 nm) topographs of native membrane proteins. Structural details unveiled are very similar to those observed using contact mode AFM.[12,15b] This, together with the comparison of PM structure and AFM topography (Figure 4) indicates that the PM was not distorted by force–volume AFM imaging. In contrast to other AFM

imaging approaches, force–volume AFM records chemical and physical information at a spatial resolution similar to the topography. Initially, the additional AFM channels recorded showed meaningless noise. However, by averaging we were able to obtain quantitative information from these channels. Mapping this additional information onto the structural model of the protein membrane (Figure 4) allows for the first time, to correlate experimentally determined chemical and physical properties. Young's modulus maps reveal the elastic properties of lipids and of BR that enable the light-driven proton pump to conduct functionally important conformational changes. Deformation maps are thought to measure the structurally deformability of soft biological samples and to determine spring constants of proteins and lipids to molecular resolution. Our experimental data suggests that electrostatic interactions contribute to the deformation measured by high-resolution force–volume AFM. How the electrostatic contribution and the structural deformability can be separated from each other must be investigated in detail. Adhesion maps detect attractive interactions between AFM tip and sample. Because the AFM tip is a multifunctional nanoscopic tool,[1] chemically functionalizing the tip will in the future allow chemical groups and their adhesive interaction forces, energies and kinetics to be mapped on protein surfaces. Probing these interactions at different time rates will provide insights into the binding kinetics and energetics of, for example, a ligand with a membrane receptor.

High-resolution force–volume AFM allows multiple chemical and physical parameters of native biological samples to be quantified and mapped at a lateral resolution approaching 1 nm. This feature will be used in the future to structurally image and to map specific chemical and physical information of native proteins and biomolecular complexes.

Experimental Section

Sample preparation: PM from *H. Salinarum* was prepared for AFM as described elsewhere.[12] Briefly, PM was adsorbed onto freshly cleaved mica in buffer solution (150 mM KCl, 10 mM Tris-HCl, pH 7.6). After 15 min of adsorption the sample was rinsed with the same buffer to remove weakly attached PMs. Then, the sample PM was imaged using AFM. Buffers were prepared using nanopure water (18 MOhm cm^{-1}) and analytical grade chemicals.

Force-volume AFM: AFM imaging was performed using a Nanoscope Multimode 8 (Bruker, Santa Barbara, USA) equipped with a 120 μm piezoelectric scanner. The 70 μm long V-shaped silicon nitride cantilevers (Bruker) had nominal spring constants of 0.4 N m^{-1} with silicon tips having a nominal apex of 2 nm. The AFM was operated in force–volume mode at a scan frequency of 0.8–1 Hz. For each pixel of the topography (512 × 512 pixels) we recorded F–D curves (Supporting Information Figure S1) at a frequency of 2 kHz over approach–retrace distances of approximately 16 nm. The maximum force (trigger force) at which the AFM tip was pushed onto the sample was limited to preset values. The trigger force could be controlled at an accuracy of ± (7–8) pN. The feedback loop controlling the AFM tip scanning the sample was adjusted to optimize for topographic resolution and minimize trigger force error. For more information see supporting information.

Received: June 10, 2011
Revised: September 7, 2011
Published online: October 17, 2011

Keywords: atomic force microscopy · bacteriorhodopsin · lipids · membrane proteins · molecular interactions

[1] a) C. Gerber, H. P. Lang, *Nat. Nanotechnol.* **2007**, *1*, 3 – 5; b) D. J. Müller, Y. Dufrene, *Nat. Nanotechnol.* **2008**, *3*, 261 – 269.
[2] a) A. Engel, D. J. Müller, *Nat. Struct. Biol.* **2000**, *7*, 715 – 718; b) J. Yu, C. A. Bippes, G. M. Hand, D. J. Muller, G. E. Sosinsky, *J. Biol. Chem.* **2007**, *282*, 8895 – 8904.
[3] D. J. Muller, A. Engel, *Curr. Opin. Colloid Interface Sci.* **2008**, *13*, 338 – 350.
[4] a) D. J. Müller, A. Engel, U. Matthey, T. Meier, P. Dimroth, K. Suda, *J. Mol. Biol.* **2003**, *327*, 925 – 930; b) H. Yamashita, K. Voitchovsky, T. Uchihashi, S. A. Contera, J. F. Ryan, T. Ando, *J. Struct. Biol.* **2009**, *167*, 153 – 158.
[5] a) P. Hinterdorfer, Y. F. Dufrene, *Nat. Methods* **2006**, *3*, 347 – 355; b) A. Engel, H. E. Gaub, *Annu. Rev. Biochem.* **2008**, *77*, 127 – 148; c) D. J. Müller, J. Helenius, D. Alsteens, Y. F. Dufrene, *Nat. Chem. Biol.* **2009**, *5*, 383 – 390.
[6] a) A. Rosa-Zeiser, E. Weilandt, S. Hild, O. Marti, *Meas. Sci. Technol.* **1997**, *8*, 1333 – 1338; b) H. J. Butt, B. Cappella, M. Kappl, *Surf. Sci. Rep.* **2005**, *59*, 1 – 152.
[7] a) M. Stark, C. Moeller, D. J. Müller, R. Guckenberger, *Biophys. J.* **2001**, *80*, 3009 – 3018; b) M. Dong, S. Husale, O. Sahin, *Nat. Nanotechnol.* **2009**, *4*, 514 – 517.
[8] J. Israelachvili, *Intermolecular & surface forces*, 2nd ed., Academic Press Limited, London, **1991**.
[9] H.-J. Butt, *Biophys. J.* **1991**, *60*, 1438 – 1444.
[10] a) M. H. J. Koch, N. A. Dencher, D. Oesterhelt, H.-J. Plöhn, G. Rapp, G. Büldt, *EMBO J.* **1991**, *10*, 521 – 526; b) T. Hirai, S. Subramaniam, J. K. Lanyi, *Curr. Opin. Struct. Biol.* **2009**, *19*, 433 – 439.
[11] J. Heberle, J. Riesle, G. Thiedemann, D. Oesterhelt, N. A. Dencher, *Nature* **1994**, *370*, 379 – 382.
[12] D. J. Müller, A. Engel, *Nat. Protoc.* **2007**, *2*, 2191 – 2197.
[13] D. J. Müller, H.-J. Sass, S. Müller, G. Büldt, A. Engel, *J. Mol. Biol.* **1999**, *285*, 1903 – 1909.
[14] B. V. Derjaguin, V. M. Muller, Y. P. Toropov, *J. Colloid Interface Sci.* **1975**, *53*, 314 – 326.
[15] a) D. J. Müller, A. Engel, *Biophys. J.* **1997**, *73*, 1633 – 1644; b) J. B. Heymann, D. J. Müller, E. Landau, J. Rosenbusch, E. Pebay-Peroulla, G. Büldt, A. Engel, *J. Struct. Biol.* **1999**, *128*, 243 – 249.
[16] D. J. Müller, D. Fotiadis, S. Scheuring, S. A. Müller, A. Engel, *Biophys. J.* **1999**, *76*, 1101 – 1111.
[17] G. Zaccai, *Science* **2000**, *288*, 1604 – 1607.
[18] D. M. Engelman, *Nature* **2005**, *438*, 578 – 580.
[19] a) H. Luecke, B. Schobert, H. T. Richter, J. P. Cartailler, J. K. Lanyi, *J. Mol. Biol.* **1999**, *291*, 899 – 911; b) J. P. Cartailler, H. Luecke, *Annu. Rev. Biophys. Biomol. Struct.* **2003**, *32*, 285 – 310.
[20] D. J. Müller, D. Fotiadis, A. Engel, *FEBS Lett.* **1998**, *430*, 105 – 111.
[21] M. Shibata, T. Uchihashi, H. Yamashita, H. Kandori, T. Ando, *Angew. Chem.* **2011**, *123*, 4502 – 4505; *Angew. Chem. Int. Ed.* **2011**, *50*, 4410 – 4413.

